Nat. Hazards Earth Syst. Sci., 14, 2803–2815, 2014
www.nat-hazards-earth-syst-sci.net/14/2803/2014/
doi:10.5194/nhess-14-2803-2014

Natural Hazards and Earth System Sciences
Open Access

Rn and CO_2 geochemistry of soil gas across the active fault zones in the capital area of China

X. Han, Y. Li, J. Du, X. Zhou, C. Xie, and W. Zhang

CEA Key Laboratory of Earthquake Prediction (Institute of Earthquake Science), China Earthquake Administration, Beijing, 100036, China

Correspondence to: Y. Li (subduction6@hotmail.com)

Received: 5 November 2013 – Published in Nat. Hazards Earth Syst. Sci. Discuss.: 20 February 2014
Revised: 6 September 2014 – Accepted: 17 September 2014 – Published: 24 October 2014

Abstract. The present work is proposed to investigate the spatiotemporal variations in soil gas Rn and CO_2 across the active faults in the capital area of China in order to understand fault activities and assess seismic hazard. A total of 342 soil gas sampling sites were measured twice in 2011 and 2012 along seven profiles and across four faults. The results of soil gas surveys show that, in each profile, due to the variation in gas emission rate, the concentrations of Rn and CO_2 changed in the vicinity of faults. Spatial distributions of Rn and CO_2 in the study areas were different from each other, which was attributed to soil types affecting the existence of Rn and CO_2. Compared with the measurement result of 2011, the increasing amplitude of average concentration value of Rn and CO_2 in profiles in 2012 ranged from 30.2 to 123.4 % and 66.3 to 131.7 %, respectively, which were coincident with the enhancement of seismic activities in the capital area of China. Our results indicate that special attention with regard to seismic monitoring should be paid to the Xinbaoan–Shacheng Fault and the northeastern segment of the Tangshan Fault in the future.

1 Introduction

Soil gas measurement has received much attention as an effective method to trace hidden faults (e.g., Baubron et al., 2002; Fu et al., 2005; Ciotoli et al., 2007; Walia et al., 2010; Al-Hilal and Al-Ali, 2010) and monitor seismic activities (e.g., Toutain and Baubron, 1999; Yang et al., 2005; Kumar et al., 2009; Walia et al., 2012). The stress/strain changes related to seismic activity may force crustal fluid to migrate up, especially along faults (King, 1986), thereby altering the geochemical characteristics of the faults. Active faults, which are composed of highly fractured rock materials, gouge and fluid, favor gas leaks from the solid earth (Toutain and Baubron, 1999; Baubron et al., 2002).

Spatiotemporal variations in soil gases at a fault zone may reflect the regional crustal stress/strain changes related to seismotectonic activity (Fu et al., 2008; Zhou et al., 2010). Lombardi and Voltattorni (2010) studied the geochemistry characteristics of Rn, He and CO_2 in soil gases in two Italian areas characterized by different seismotectonic activity, and found that, due to seismic activity favoring gas migration from the deep, the concentrations of soil gases were much higher in Colpasquale (a seismically active region) than the Campidano Graben, which is characterized by seismic quiescence. Before earthquakes, a sharp increase in soil Rn concentration in both sites, which are separately located in active and non-active tectonic zone of West Bengal, was reported by Ghosh et al. (2011), but the average radon concentration was much higher in the Jalpaiguri site, which is located in an area of active tectonics, compared to the Kolkata site with non-active tectonic zone. Camarda et al. (2012) analyzed the relationship between soil CO_2 emission and Mt. Etna volcanic activity. The result implies that the anomalous degassing of CO_2 can be mainly controlled by migration of fresh magma from deep to shallow portions of the Etna plumbing system. Therefore, the enhanced tectonic activity favors the uprising of significant gas deep in the earth and consequently causes an increase in soil gas concentration.

The capital area of China (38.7–41.3° N, 114.1–119.9° E) is a densely populated and economically developed region which consists of Beijing, Tianjin, Zhangjiakou and Tangshan, among others (Fig. 1). Its seismicity, which is mainly

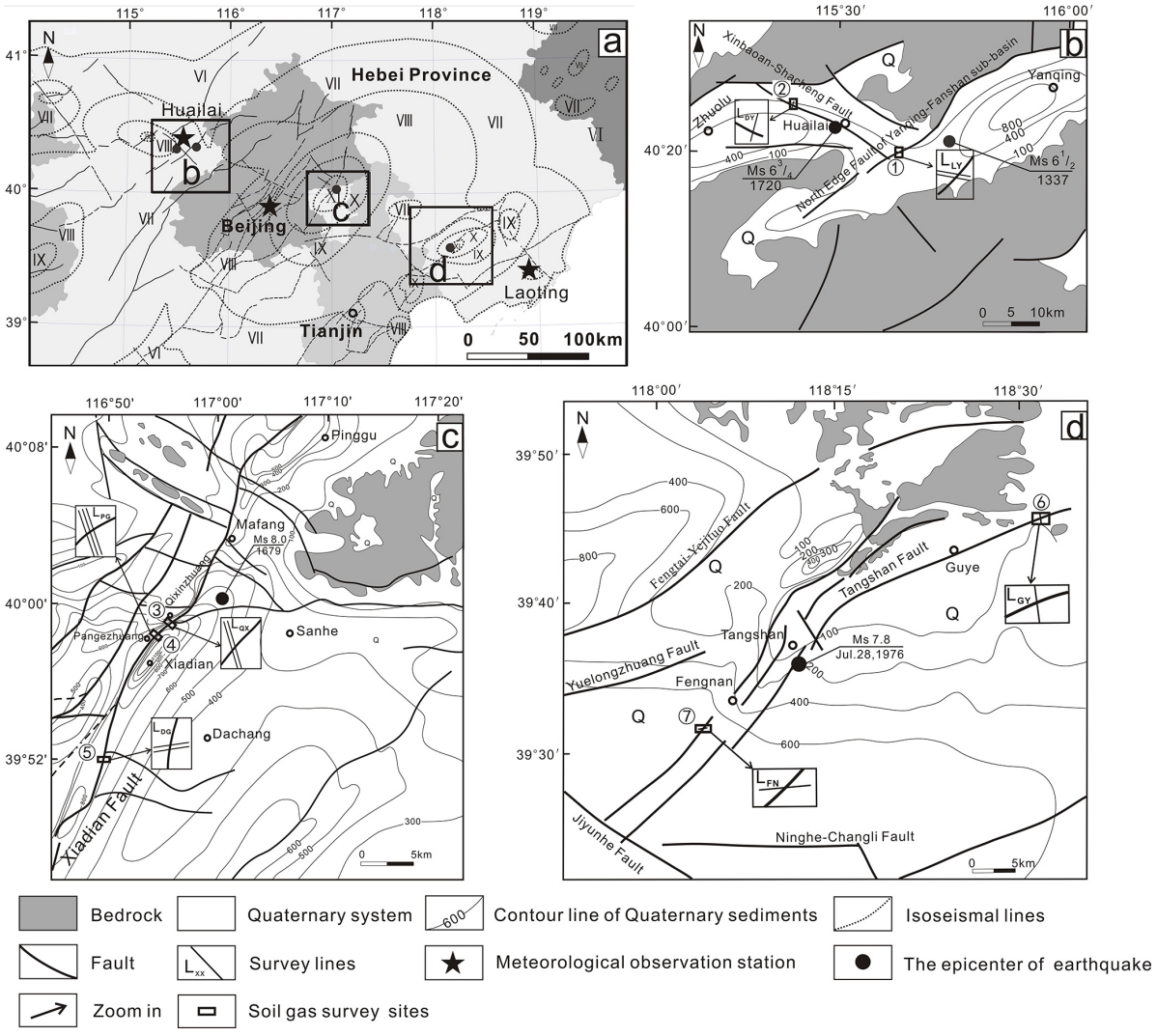

Figure 1. Simplified geological maps of study areas in the capital area of China (modified after Zhu et al., 2006; Seismic Geological Brigade, CEA, 1979; Yin, 2010; Guo et al., 2011). **(a)** shows the locations of study areas and meteorological observation stations. **(b–d)** show the geologic structure and locations of soil gas profiles in Yanqing–Huailai Basin, the Sanhe–Pinggu region and the Tangshan region, respectively. ① represents the LY profile, ② the DY profile, ③ the QX profile, ④ the PG profile, ⑤ the DG profile, ⑥ the GY profile, and ⑦ the FN profile (full names of profiles provided in the text).

controlled by hidden active faults, is high (Gao and Ma, 1993), particularly in Yanqing–Huailai Basin and the Sanhe–Pinggu and Tangshan regions. In Yanqing–Huailai Basin, several earthquakes greater than $M_S = 6.0$ have occurred, and 163 events greater than $M_S = 2.0$ were recorded there between 1970 and 2004 (Zhu et al., 2006). In the Sanhe–Pinggu region, four paleoearthquake events, including the 1679 $M_S = 8.0$ earthquake, have been identified that occurred within the last 20 000 years, and they showed quasi-periodic occurrence (Ran et al., 1997). In the Tangshan area, the 1976 $M_S = 7.8$ Tangshan earthquake occurred, causing 242 000 deaths (State Seismological Bureau, 1982). As soil gases can be tracers for seismotectonic activities, soil gas investigations in the capital area of China are very important for the understanding of fault activities and the assessment of seismic hazard.

Soil gas surveys in the capital area have been carried out by some researchers since the 1990s. Wang et al. (2014) analyzed the relationship between soil gas Rn and the seismogenic faults in the Tangshan area and found that higher Rn concentrations mainly appeared in faults where large earthquakes had occurred. Li et al. (2009) discussed the geochemical characteristics of soil gases in Yanqing–Huailai Basin and found that the concentrations of Rn, CO_2, He, H_2 and Hg were higher in the east of the basin than the west, which may be related to the tectonic activity of the area. Li et al. (2013) investigated the concentrations of soil gases (Hg, Rn, H_2, He and CO_2) in the Tangshan region and identified that the

gaseous anomalies are consistent with the trace of the Tangshan faults. Though soil gas investigations in the capital area have been made and some gratifying achievements have been obtained, the difference in fault activities in the capital area has seldom been systematically investigated by means of soil gas survey.

This work is proposed to study the spatiotemporal variations of soil gases across different faults in the capital area of China in order to understand fault activities and assess seismic hazard through measurements of soil gas Rn and CO_2.

2 Seismotectonic settings

The capital area is located in the north of northern China. Its tectonic setting is complex, containing within it the Yanshan–Yinshan uplift, the Taihang–Wutai uplift and the North China Basin. The area is vulnerable to intense seismicity caused by numerous faults oriented in the NE–SW direction (Xu et al., 2002). Low-velocity and high-conductivity anomalies, which may be related to fluids, have been observed in the area of the lower crust to the uppermost mantle below the foci of large earthquakes, such as the 1976 $M_S = 7.8$ Tangshan earthquake and the 1679 $M_S = 8.0$ Sanhe–Pinggu earthquake (Huang and Zhao, 2004). Consequently, the seismogenic layer in the upper and middle crust may be weakened by the fluids in the lower crust, which may trigger large crustal earthquakes (Huang and Zhao, 2004).

2.1 Yanqing–Huailai Basin

Yanqing–Huailai Basin, including Yanqing–Fanshan sub-basin and Huailai–Zhuolu sub-basin, is located in the North China Plain and the northeastern edge of the Shanxi Rift (Fig. 1a and b). The tectonic environment in the basin is complicated due to the coupling interaction between the Yinshan–Yanshan orogenic belt and the Shanxi Rift. The North Edge Fault of Yanqing–Fanshan sub-basin (NEYF Fault), the largest active normal fault in Yanqing–Huailai Basin, is a 102 km long northeastward-trending fault, dipping towards SE at an angle of 55–80°(Gao and Ma, 1993). The Xinbaoan–Shacheng Fault, intersecting with the NEYF Fault, is 26 km long in a 290° trend and dips towards SW at an angle of 65 to 75° (Gao and Ma, 1993). Earthquakes above $M_S = 6.0$ have occurred in the region, including the 1337 $M_S = 6.5$ Langshan earthquake and the 1720 $M_S = 6.7$ Shacheng earthquake (Earthquake Disaster Defense Department of CEA, 1995; Fig. 1b).

The basements of Yanqing–Huailai Basin are composed of Archaean metamorphic rocks, Proterozoic and Paleozoic dolomites, gneisses and clastic rocks, interbedded with thin layers of coal as well as Mesozoic intermediate-basic to acid volcanics and pyroclastics. The Pliocene sediments mainly consist of grey cemented gravels which were overlaid unconformably by the Pleistocene sediments, including fluvial and lacustrine sand, gravel, silt and clay (Pavlides et al., 1999).

2.2 Xiadian Fault

The seismic area of the 1679 $M_S = 8.0$ Sanhe–Pinggu earthquake is located at the intersection of the Yinshan–Yanshan uplift and subsiding belt of the North China Plain (Zhang et al., 2002; Fig. 1c). The Xiadian Fault, the seismogenic structure of the 1679 earthquake, is an important buried fault in the north of the North China Plain, dipping in the range of 50–70° with a NE strike (Xu et al., 2000). The Quaternary strata in the Sanhe–Pinggu region are mainly composed of clay, sand and aleurite (Jiang et al., 2000).

2.3 Tangshan Fault

The Tangshan region, close to the north of the North China Plain and located on the southern edge of the Yanshan uplift, is known as a "rhombic block" and is surrounded by four large faults (Fig. 1a). The Tangshan Fault, the seismogenic structure of the 1976 $M_S = 7.8$ Tangshan earthquake, located along the diagonal of the "rhombic block", consists of several NE strike segments with high dip angles and right-lateral slip (Fig. 1d). A fault slip rate of 2.6 mm yr^{-1} at 15 km depth was obtained from the analysis of the repeating of seismic events observed along the Tangshan Fault. This is better explained by the article of Li et al. (2007), that repeating earthquakes are a series of earthquakes regularly occurring on a patch of a fault plane.

3 Methodology

Rn and CO_2 were sampled by inserting a hollow stainless steel sampler with a diameter of 3 cm into the ground down to a depth of 80 cm. The sampler was connected to a radon detector through rubber tubes. Radon measurement was performed in the field using a RAD7 radon detector. In brief, the RAD7 detector counts the α particles emitted during the decay of ^{222}Rn to ^{218}Po. It takes 15 min for radon analysis at each sampling site for three measuring cycles. The sensitivity and measurement error of the radon detector are 14.8 Bq m^{-3} and ±5 %, respectively (Zhou et al., 2010). Soil gas CO_2 was analyzed by using an Agilent 3000 gas chromatograph (GC) equipped with a thermal conductivity detector (TCD), with a measurement error of ±5 %. Soil gas CO_2 sampled from the sampling device was immediately injected into the GC via a glass syringe. The detection limit of CO_2 is 2 ppm, calibrated by standard gas (Li et al., 2009, 2013).

Soil gas surveys were carried out twice during August to September 2011 and September to October 2012. Meteorological parameters in the first soil gas survey were similar to those in the second soil gas survey (Fig. 2). Monthly average values of air temperature, air humidity, wind speed and barometric pressure were based on daily average values,

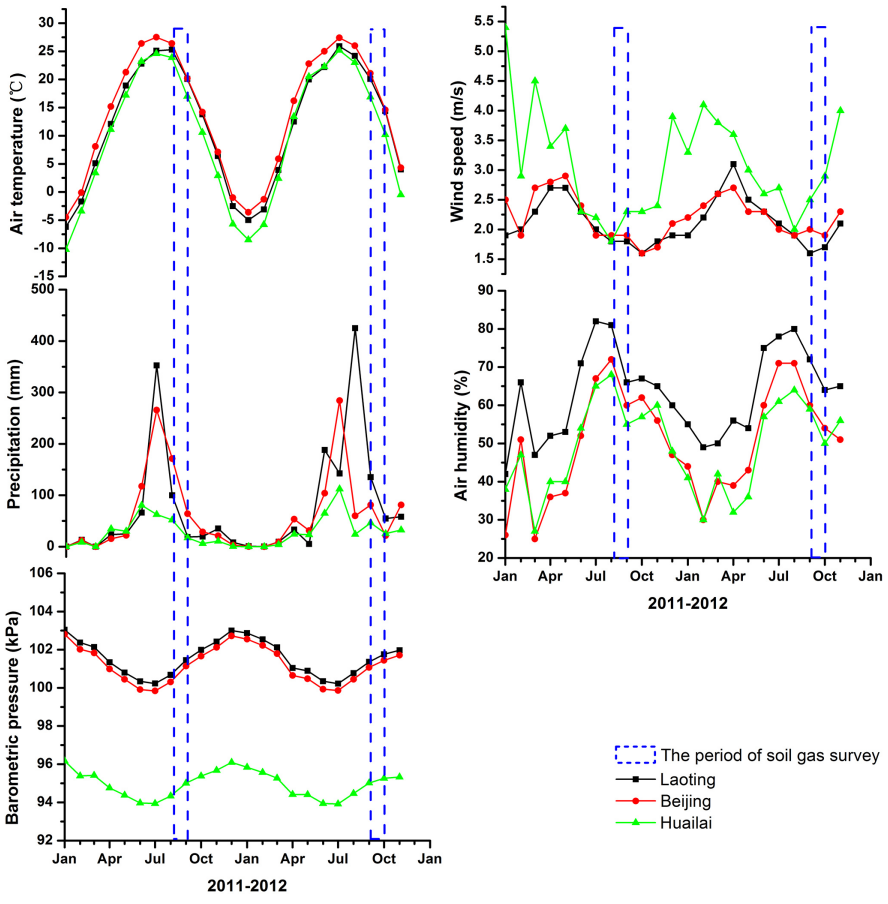

Figure 2. Monthly average values of meteorological parameters in the capital area of China, from January 2011 to November 2012 (China Meteorological Data Sharing Service System, http://cdc.cma.gov.cn/home.do). The black lines represent meteorological parameters in Laoting county, Tangshan region; the red lines represent meteorological parameters in Beijing, which is close to the Sanhe–Pinggu region; the green lines represent meteorological parameters in the Huailai area, Yanqing–Huailai Basin; the blue dotted lines represent the period of soil gas surveys.

which were computed using the observation data at 2.00 a.m., 8.00 a.m., 14.00 p.m. and 20.00 p.m. The values of monthly precipitation were based on accumulation of daily precipitation. The detection limits of precipitation, air temperature, air humidity, wind speed and barometric pressure are 0.1 mm, 0.1°, 1 %, 0.1 m s^{-1} and 0.1 hPa, respectively. The locations of meteorological observation stations can be found in Fig. 1a (black star).

The soil gases were sampled along the measuring line at a distance of 20 m, and the distance between the two parallel measuring lines was 5 m. In Yanqing–Huailai Basin, 50 and 33 sampling sites of soil gases were measured, respectively, at the village of Laoyingwa (LY) along two parallel measuring lines across the NEYF Fault and at the village of Daying (DY) along one measuring line across the Xinbaoan–Shacheng Fault (Fig. 1b). In the Sanhe–Pinggu region, a total of 188 sampling sites of soil gases were measured at Qixinzhuang (QX), Pangezhuang (PG) and Dadongguan (DG) villages along three profiles across Xiadian Fault (Fig. 1c). A total of 66 and 50 sampling sites of soil gases along two parallel measuring lines were separately arranged at the QX and DG profiles, and 72 sampling sites of soil gases along three parallel measuring lines were arranged at the PG profile. In the Tangshan region, 48 and 23 sampling sites of soil gases were measured along the Guye (GY) measuring line and the Fengnan (FN) measuring line across the Tangshan Fault, respectively (Fig. 1d).

4 Results and discussion

4.1 Spatiotemporal distributions of Rn and CO_2

Measurement results of soil gas Rn and CO_2 are listed in Fig. 3. The statistical anomaly threshold value of soil gas could be influenced by various factors, such as tectonics, lithological characteristics, seasonal variations and anthropogenic factors. The heterogeneity of bedrock, tectonics and soil thickness leads to variations in the anomaly threshold of

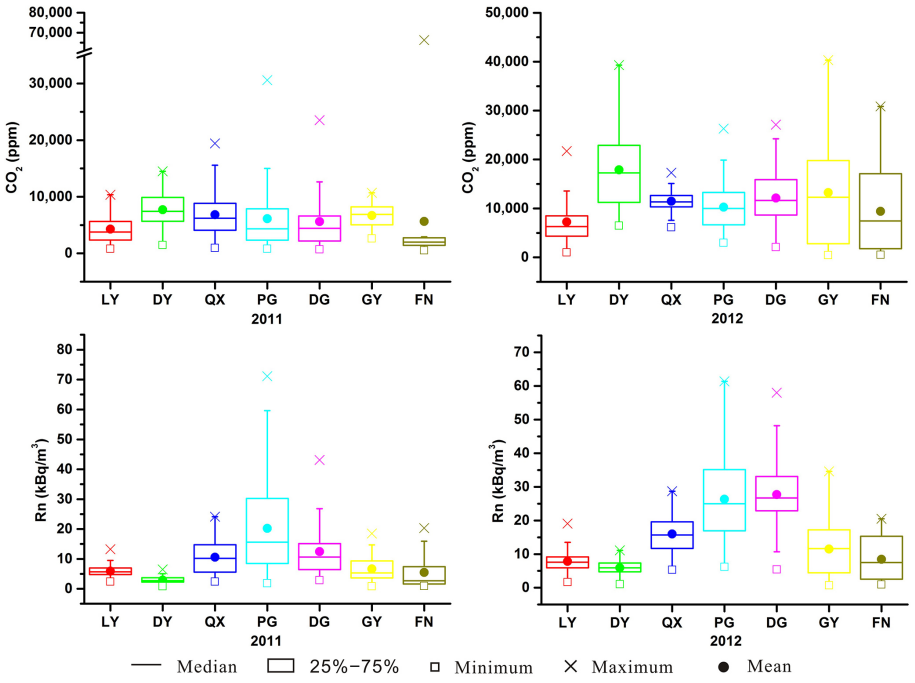

Figure 3. Box plots of Rn and CO_2 over the two surveys in the capital area of China.

soil gas in the study area, one such occurrence being granite having significant effects on the values of the anomaly threshold of soil gas Rn (Choubey et al., 1999). The statistical anomaly threshold value of soil gas may be determined by means of several methods, such as a cumulative probability (or $Q-Q$) plot (Ciotoli et al., 2007; Zhou et al., 2010), the mean plus n time the standard deviation (SD) (Ciotoli et al., 1998; Fu et al., 2005; Walia et al., 2008; Al-Hilal and Al-Ali, 2010) and empirical data distribution (Seminsky and Demberel, 2013).

In the present study, the amount of sampling sites in some profiles is insufficient for use in the method of cumulative probability plots. The empirical data of soil gas Rn and CO_2 in the study areas are not systematically determined. In this work, the anomaly threshold values of Rn and CO_2 were determined using the method of mean + SD for soil gas data that obey normal distribution. As for those of non-normal distribution, extremely high and low gas values in the profile, which may provide non-representative statistical parameters and perturb the real anomalies, were excluded. For the statistics, 5 % data points with extremely high values and 5 % data points with low values are excluded from the data set, respectively. Hence, the trimmed sample set could obey normal distribution and the anomaly threshold values were calculated via mean + SD of the trimmed sample set. As for the density function of normal distribution, the credibility of the anomaly threshold values selected as mean + SD is established by a probability of 84.1 % (Elkins, 1940). Therefore, soil gas values greater than mean + SD could be regarded as true anomalies. The soil gas values, except Rn at the PG profile in 2011 and the LY profile in 2012 and CO_2 at the PG profile in 2011, the DG profile in 2011 and the FN profile in 2011, obey normal distribution (significance < 0.05 in Kolmogorov–Smirnov test).

Figure 4 shows the distributions of Rn and CO_2 along two parallel measuring lines, LYI and LYII (5 m between the two parallel measuring lines), across the NEYF Fault. In the LY profile, Rn varies from 2.4 to 13.2 kBq m^{-3} and 1.7 to 19.1 kBq m^{-3} in the 2011 and 2012 soil gas surveys, respectively; CO_2 ranges from 806.0 to 10 345.0 ppm and from 1005.3 to 21 697.8 ppm in the 2011 and 2012 soil gas surveys, respectively. Anomalously high concentrations of Rn and CO_2 along the two measuring lines can be found near the NEYF Fault (Fig. 4). However, both Rn and CO_2 did not show high concentrations on the fault, which may imply that the fault contains gouge and ultracataclasite with a low permeability. Spatial distributions of Rn and CO_2 along the two profiles show that the increase in CO_2 during the period of soil gas investigations was greater than that of Rn (Fig. 4).

The measurement results of Rn and CO_2 along the DY profile show that Rn and CO_2 concentrations increased sharply in 2012 compared with 2011, especially from 320 to 640 m along the profile, which was located on the hanging wall of the fault (Fig. 5). The variations in Rn and CO_2 are attributed to the geological factors, especially fault activity.

In the Sanhe–Pinggu region, Rn and CO_2 were sampled along three profiles across the Xiadian Fault (Fig. 1c). In the two soil gas surveys, the average concentration of CO_2 at the QX, PG and DG profiles varies from 6828.2 to 11 467.2, 6123.0 to 10 273.1, and 5609.6 to 12 119.9 ppm, respectively;

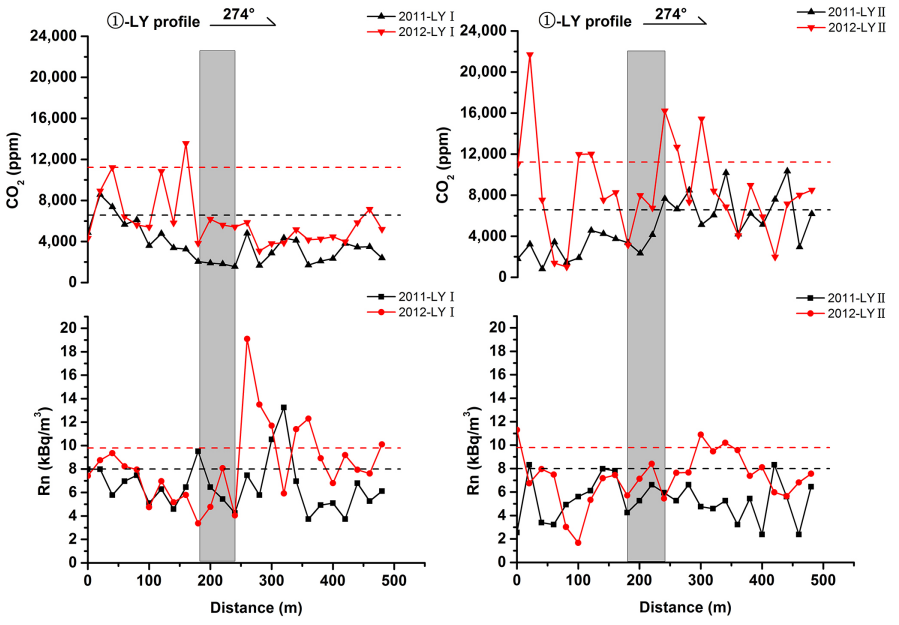

Figure 4. Rn and CO_2 concentrations along the LY profile across the NEYF Fault. The shaded bar represents the location of the fault. The black and red dotted lines represent the anomaly threshold of soil gas in 2011 and 2012, respectively. The arrow at the top (with number above) represents the direction of the profile.

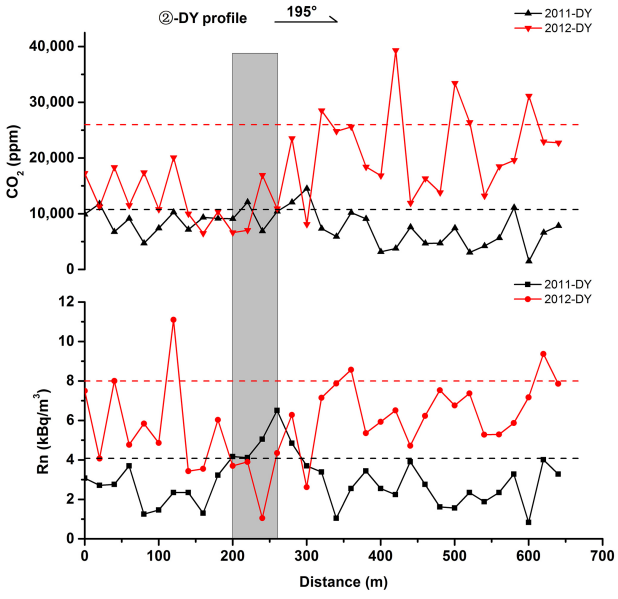

Figure 5. Rn and CO_2 concentrations along the DY profile across the Xinbaoan–Shacheng Fault. The shaded bar represents the location of the fault. The black and red dotted lines represent the anomaly threshold of soil gas in 2011 and 2012, respectively. The arrow at the top (with number above) represents the direction of the profile.

the average concentration of Rn at the QX, PG and DG profiles ranges from 10.4 to 16.0, 20.2 to 26.3, and 12.4 to 27.7 kBq m^{-3}, respectively. It is worth noting that the concentrations of CO_2 and Rn both increased at these profiles, but the increase in CO_2 and Rn at the DG profile is greater than at the QX and PG profiles, particularly the increase in Rn. This indicates that variations in Rn and CO_2 may be caused by regional crustal stress/strain changes. The inhomogeneous leakage of Rn and CO_2 occurs on the Xiadian Fault (Figs. 6, 7 and 8). The sampling sites with anomalously high concentrations of soil gas were located at isolated points known as gas vents on the Xiadian Fault, but the ones with low concentrations were located in low-permeability zones on the fault (Annunziatellis et al., 2008). It implies inhomogeneous leakage caused by permeability heterogeneity along the Xiadian fault zone. At some sampling sites, the anomalous concentrations of Rn and CO_2 do not always match each other. This suggests that the source of Rn and CO_2 at the sampling site for the deep source component has high values of Rn and CO_2 and the shallow source component has high CO_2 but low Rn concentrations.

Figure 9 shows the distributions of Rn and CO_2 along the GY profile across the Tangshan Fault. In the two soil gas investigations, the maximum concentrations of Rn and CO_2 at the GY profile increased from 18.5 to 34.6 kBq m^{-3} and 10 706.2 to 40 315.5 ppm, respectively. The anomalies of Rn and CO_2 along the GY profile in 2012 soil gas survey present irregular shapes. This may be related to the seismicity in the Tangshan region, which will be discussed in a later section. Spatial distributions of Rn and CO_2 along the FN profile show double peak anomalies (Fig. 10), which implies that the Tangshan faults were mature faults with fault cores and damage zones (Annunziatellis et al., 2008). Fault cores composed

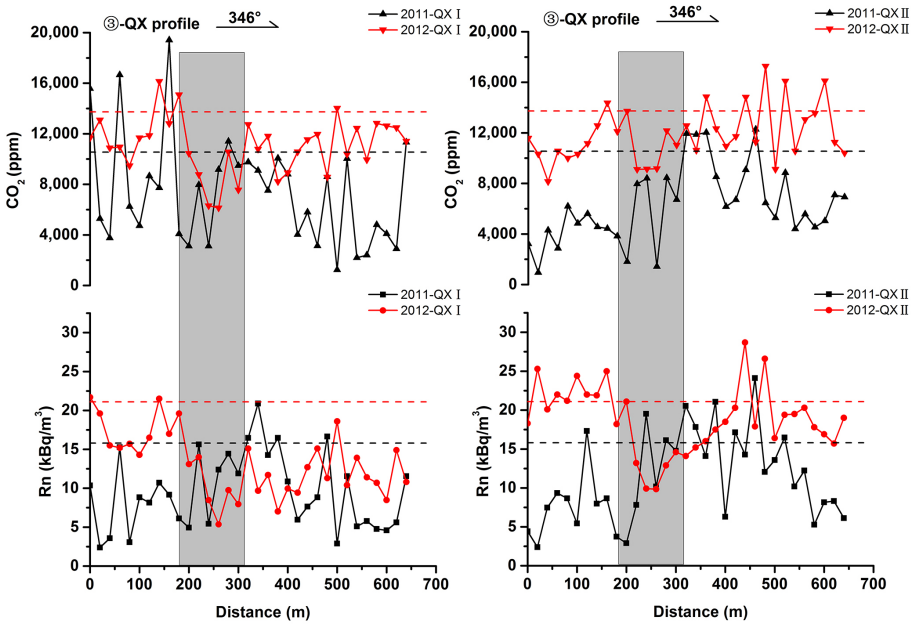

Figure 6. Rn and CO_2 concentrations along the QX profile across the Xiadian Fault. The shaded bar represents the location of the fault. The black and red dotted lines represent the anomaly threshold of soil gas in 2011 and 2012, respectively. The arrow at the top (with number above) represents the direction of the profile.

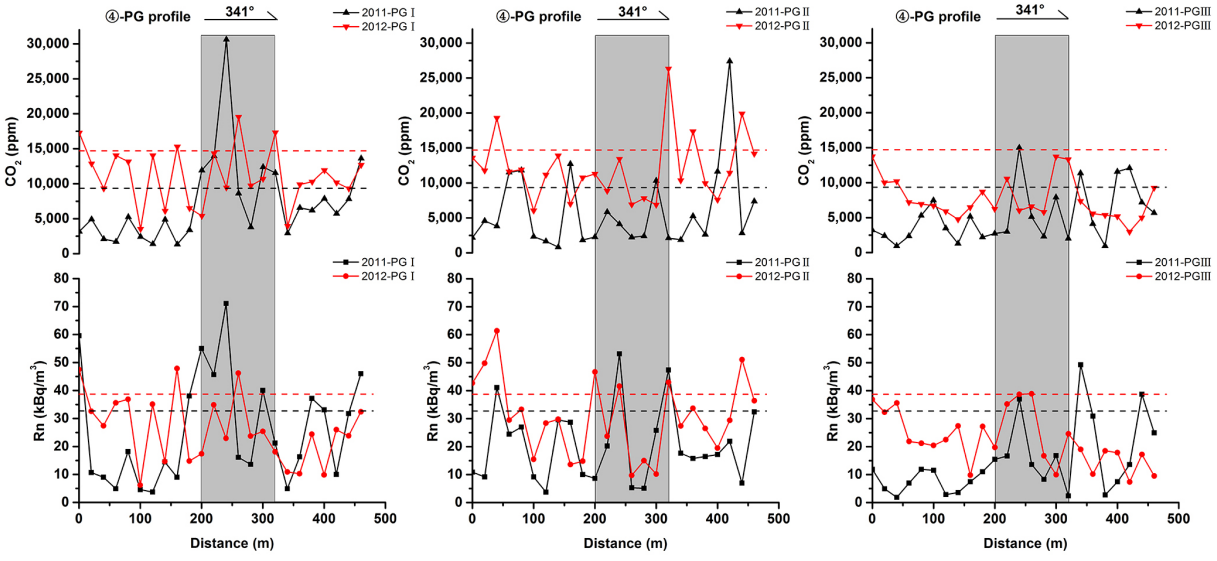

Figure 7. Rn and CO_2 concentrations along the PG profile across the Xiadian Fault. The shaded bar represents the location of the fault. The black and red dotted lines represent the anomaly threshold of soil gas in 2011 and 2012, respectively. The arrow at the top (with number above) represents the direction of the profile.

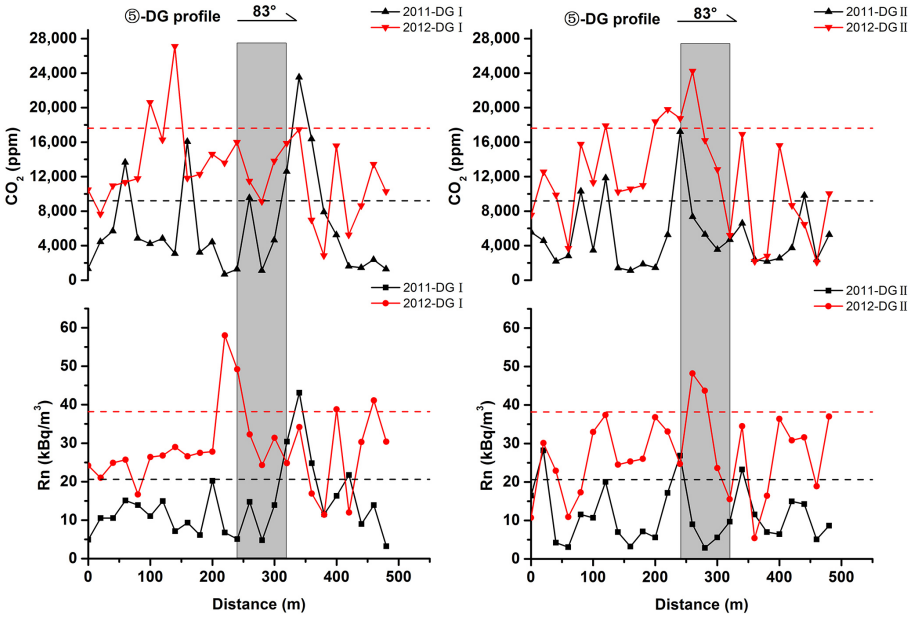

Figure 8. Rn and CO_2 concentrations along the DG profile across the Xiadian Fault. The shaded bar represents the location of the fault. The black and red dotted lines represent the anomaly threshold of soil gas in 2011 and 2012, respectively. The arrow at the top (with number above) represents the direction of the profile.

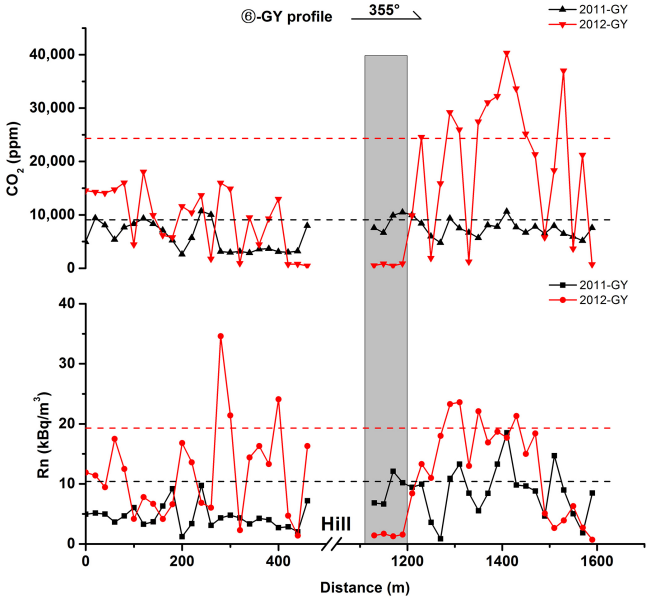

Figure 9. Rn and CO_2 concentrations along the GY profile across the Tangshan Fault. The shaded bar represents the location of the fault. The black and red dotted lines represent the anomaly threshold of soil gas in 2011 and 2012, respectively. The arrow at the top (with number above) represents the direction of the profile.

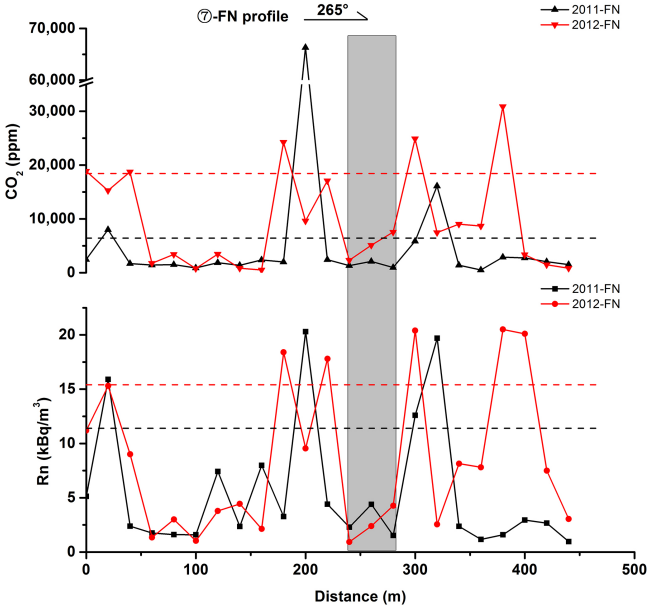

Figure 10. Rn and CO_2 concentrations along the FN profile across the Tangshan Fault. The shaded bar represents the location of the fault. The black and red dotted lines represent the anomaly threshold of soil gas in 2011 and 2012, respectively. The arrow at the top (with number above) represents the direction of the profile.

of gouge and ultracataclasite with a low permeability prevent migration of gas from deep in the earth up to surface, but the damage zones with high permeability favor the uprising of deep-sourced gases (Annunziatellis et al., 2008; Faulkner et al., 2010). Compared with the soil gas survey in 2011, the concentrations of Rn along the FN profile in 2012 changed slightly, whereas the concentrations of CO_2 increased.

4.2 Fault activities

The concentrations of soil gas can be affected by seismotectonic activity, rock types, porosity and composition of soil, meteorological parameters (e.g., temperature, precipitation and air moisture) and structural type (Hinkle, 1994; Toutain and Baubron, 1999; Fu et al., 2005, 2008; Walia et al., 2008; Lombardi and Voltattorni, 2010; Zhou et al., 2010). As meteorological parameters varied slightly between the two soil gas surveys (Fig. 2), the concentration variations in Rn and CO_2 at the same sampling site were mainly controlled by stress/strain changes related to seismotectonic activity. In order to compare the activities of faults in the study area, the average concentration ratio (ACR), the maximum concentration ratio (MCR) and the median concentration ratio (MEDCR) of soil gas were proposed in order to avoid the other factors influencing the gas concentrations. ACR, MCR and MEDCR can be calculated with the following Eqs. (1)–(3):

$$\mathrm{ACR} = Q_{\mathrm{ave}}[2012]/Q_{\mathrm{ave}}[2011], \quad (1)$$

where Q_{ave} [2012] is the average concentration of soil gas at one profile in 2012, and Q_{ave} [2011] is the average concentration of soil gas at the corresponding profile in 2011;

$$\mathrm{MCR} = Q_{\mathrm{max}}[2012]/Q_{\mathrm{max}}[2011], \quad (2)$$

where Q_{max} [2012] is the maximum concentration of soil gas at one profile in 2012, and Q_{max} [2011] is the maximum concentration of soil gas at the corresponding profile in 2011;

$$\mathrm{MEDCR} = Q_{\mathrm{med}}[2012]/Q_{\mathrm{med}}[2011], \quad (3)$$

where Q_{med} [2012] is the median concentration of soil gas at one profile in 2012, and Q_{med} [2011] is the median concentration of soil gas at the corresponding profile in 2011.

The ACRs, MCRs and MEDCRs of Rn and CO_2 are illustrated in Fig. 11a–c. The ACRs of Rn and CO_2 at the DY and DG profiles are greater than 2.0; the MCRs of Rn and CO_2 at the GY profile are greater than the other profiles; and the MEDCRs of Rn and CO_2 at the DY, DG and FN profiles are greater than 2.0. As the ACRs, MCRs and MEDCRs of Rn and CO_2 at the DY profile are greater than at the LY profile, this may imply that the activity of the Xinbaoan–Shacheng Fault is more intense than that of the NEYF Fault. The ACRs, MCRs and MEDCRs of Rn and CO_2 at the QX and PG profiles are less than that at the DG profiles, which may indicate that the southern segment of the Xiadian faults is more active than the middle segment. As the ACRs and MCRs of Rn and CO_2 at the GY profile are greater than the FN profile, this may suggest the activity of the northeastern segment of Tangshan Fault is more intense than the southwestern segment.

The anomaly thresholds of Rn and CO_2 have increased at different levels in the second measurement (Fig. 11d–e), indicating an enhanced emanation rate and flux of soil gases in the area. The soil gas concentration is sensitive to the stress accumulation and tectonic activity in the crust (Fu et al., 2008; Zhou et al., 2010). In general, an earthquake is a direct result of enhanced tectonic activity and underground stress accumulation. The permeability of pathways is increased by the enhanced seismic activities, resulting in more significant gas migrating to the surface (Lombardi and Voltattorni, 2010). In 2012, a total of 221 earthquakes ($M_{\mathrm{L}} \geq 1.8$) were recorded in the capital area by the China Earthquake Data Center, whereas 131 earthquakes ($M_{\mathrm{L}} \geq 1.8$) were recorded in the area in 2011 (Fig. 12, http://data.earthquake.cn/data/). Consequently, the enhanced Rn and CO_2 can be explained by the more intensive earthquake activity in the area, which led to the formation of more pathways for gas migration.

The seismic activity in the northeastern segment of the Tangshan faults is more intense than the southwestern segment, as evidenced by 99 earthquakes ($M_{\mathrm{L}} \geq 1.8$) that occurred in the northeastern segment during the years of 2011 and 2012, compared with 15 earthquakes ($M_{\mathrm{L}} \geq 1.8$) in the southwestern segment (http://data.earthquake.cn/data/). The seismic activity may coincide with the inference from the results of soil gas surveys in the Tangshan region. The irregularly shaped diffuse anomalies of Rn and CO_2 along the profile GY in 2012 soil gas survey may be related to the $M_{\mathrm{S}} = 4.7$ earthquake (28 May 2012) and the $M_{\mathrm{S}} = 3.7$ earthquake (29 May 2012, http://data.earthquake.cn/data/). New fractures were formed by the two seismic events, and the structures became more permeable, resulting in the increase in Rn and CO_2 concentrations.

4.3 The difference of spatial distributions in the study areas

The concentrations of Rn in the Sanhe–Pinggu region (QX, PG and DG profiles), the Tangshan region (GY and FN profiles) and Yanqing–Huailai Basin (LY and DY profiles) showed a descending tendency (Fig. 11f). The concentrations of Rn in Yanqing–Huailai Basin should be higher compared with the Sanhe–Pinggu and Tangshan regions, as the basements of Yanqing–Huailai Basin contain acid volcanics and pyroclastics (Pavlides et al., 1999). However, the values of Rn at the DY and LY profiles were not higher; in fact they were even lower than the Sanhe–Pinggu and Tangshan regions. The greater porosity of sandy soil (Table 1) and the

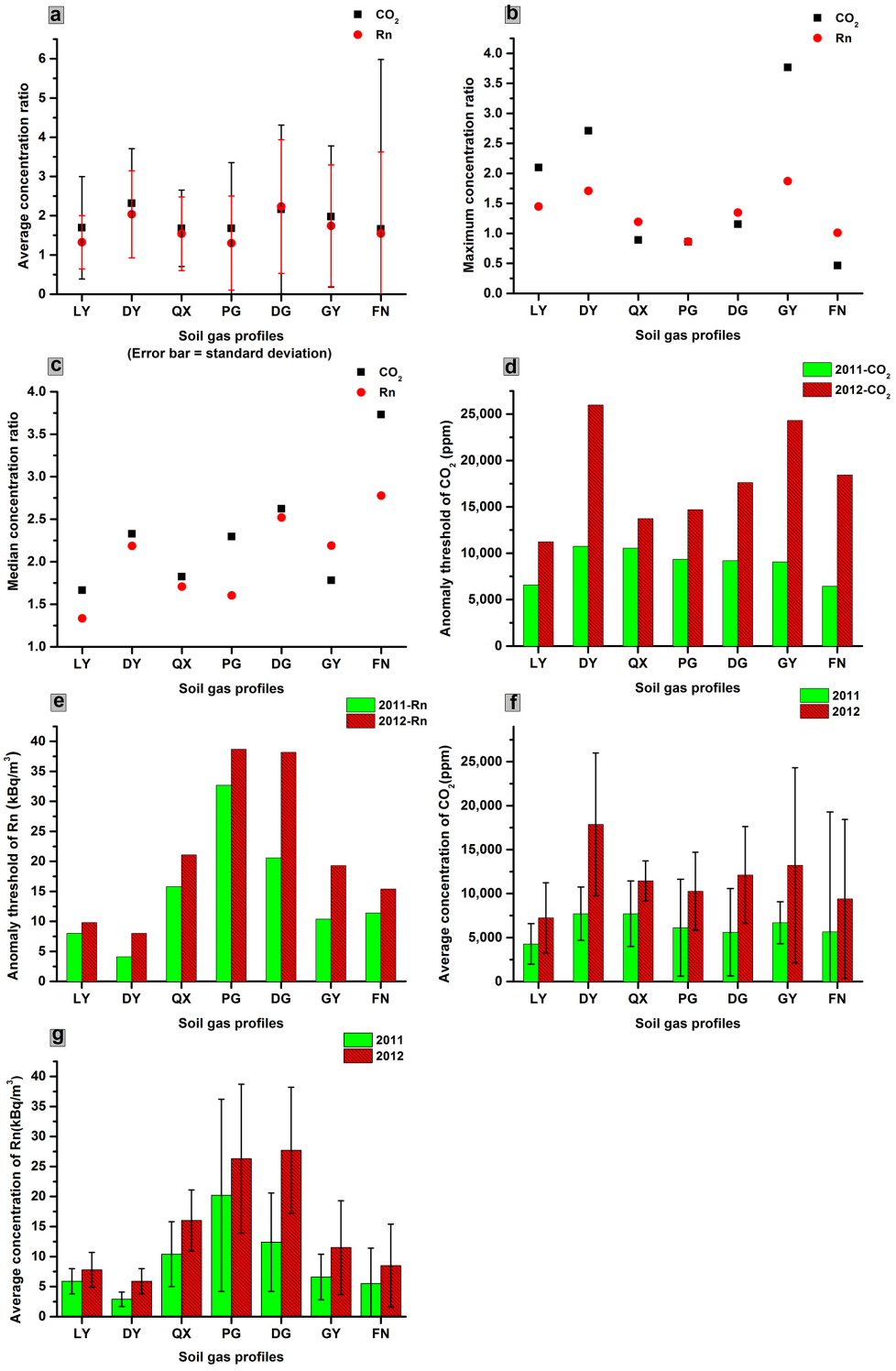

Figure 11. Spatiotemporal variations in soil gases across fault zones in the capital area of China. The profile order used along the *x* axis was based on the profile number in Fig. 1. **(a–c)** show the ratios that the average, maximum and median concentrations of soil gases at one profile in the 2012 soil gas survey were divided by that at the corresponding profile in the 2011 soil gas survey, respectively. **(d, e)** show the anomaly thresholds of Rn and CO_2 at different profiles in the 2011 and 2012 soil gas surveys. **(f, g)** show the average concentrations of Rn and CO_2 at different profiles in the 2011 and 2012 soil gas surveys. Error bars represent ± 1 standard deviation.

Table 1. Component percentages in soil in the study areas (FAO/IIASA/ISRIC/ISSCAS/JRC, 2012).

		Topsoil (0–30 cm)						Subsoil (30–100 cm)					
Profile	Soil unit name (FAO 90)	Sand fraction (%)	Silt fraction (%)	Clay fraction (%)	Gravel content (%)	Organic carbon (% weight)	USDA texture classification	Sand fraction (%)	Silt fraction (%)	Clay fraction (%)	Gravel content (%)	Organic carbon (% weight)	USDA texture classification
LY	Salic Fluvisols	37	46	17	4	0.42	loam	37	42	21	8	0.47	loam
DY	Cumulic Anthrosols	90	6	4	10	2.41	sand	89	6	5	10	0.88	sand
QX	Calcaric Cambisols	36	43	21	6	0.65	loam	34	43	23	10	0.43	loam
PG	Calcaric Cambisols	36	43	21	6	0.65	loam	34	43	23	10	0.43	loam
DG	Calcaric Cambisols	36	43	21	6	0.65	loam	34	43	23	10	0.43	loam
GY	Gleyic Luvisols	47	29	24	5	0.83	loam	39	27	34	6	0.28	clay loam
FN	Calcic Gleysols	41	40	19	4	1.3	loam	44	37	19	5	0.44	loam

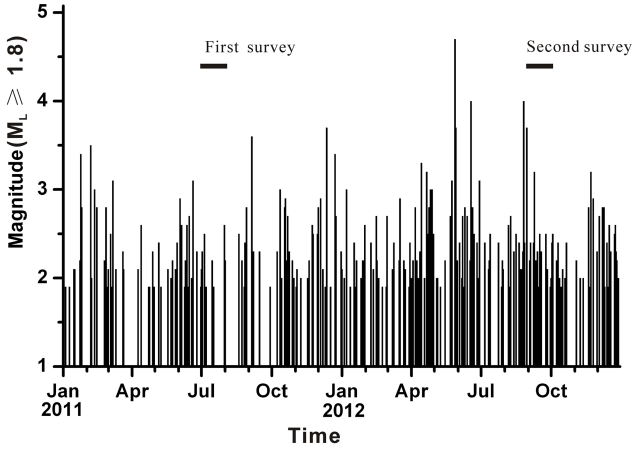

Figure 12. The earthquakes as a function of time for 2011 and 2012 in the capital area of China. The graph shows the local magnitudes for all earthquakes with $M_L \geq 1.8$, as a function of day of occurrence, from 1 January 2011 to 31 December 2012 (data from China Earthquake Data Center, http://data.earthquake.cn/data/).

lower amount of precipitation (Fig. 2) in Yanqing–Huailai Basin favor gas exchange between soil gas and air. The soil with greater porosity could present lower Rn values for dilution by atmospheric air (Fu et al., 2005). Less rainfall could result in decreased moisture content in soil and rocks, and thus the amount of emanated Rn migrating into soil pores decreased (King, 1986). Furthermore, as crustal thickness in Yanqing–Huailai Basin is larger than at the other two regions (Wang et al., 2009), the soil gas at the DY and LY profiles would contain less deep gas of Rn for the decay of ^{222}Rn to ^{218}Po with migration. Compared with the Sanhe–Pinggu region, lower values of Rn in Tangshan are affected by the high soil moisture attributed to the low ground water level (Li et al., 2013). The emanation coefficient of Rn will decrease when the moisture content of soil increases and reaches saturated conditions (Menetrez and Mosley, 1996).

However, the soil CO_2 accumulation in Yanqing–Huailai Basin and the Sanhe–Pinggu and Tangshan regions is different to that of Rn (Fig. 11g). The average concentrations of CO_2 in the study areas show a slight difference, except for CO_2 at the DY(2012) profile, where the aseismic fault slip may cause a sharp increase in the concentrations of CO_2 (Fig. 11g). This phenomenon may be attributed to different soil types in the study areas (Table 1). Gal et al. (2011) studied the relationship between soil gas behavior and soil types and discovered that coarse-grained soil is in favor of the storage of CO_2 and fine-grained clayey soil is in favor of the storage of Rn. The topsoil and subsoil at the DY profile are both sandy in composition with a high permeability, which favors gas exchange between soil gas and air. However, the average values of CO_2 in the DY profile are slightly higher than the other profiles due to the oxidation of soil organic carbon (SOC) with higher content (Table 1). The decomposition rate of organic material in soil is equal to the supply rate under natural conditions, and the content of organic material in soil is constant (Buringh, 1984). More CO_2 could release into the soil pores as SOC with higher content is oxidated. In other profiles, the average concentrations of CO_2 show a slight difference for different soil types, although the content of SOC and the fraction of sand, silt and clay in soil are similar to each other.

5 Conclusions

The spatiotemporal variations of Rn and CO_2 in soil gas in seismically active areas of the capital area of China were studied based on two soil gas surveys performed at 342 sampling sites. As meteorological parameters varied slightly between the two soil gas surveys, the increases in Rn and CO_2

concentrations in the 2012 soil gas survey may be related to the enhancement of seismic activities in the capital area of China. The average concentrations of Rn and CO_2 increased in all profiles between 2011 and 2012, ranging from 30.2 to 123.4 % and 66.3 to 131.7 % for Rn and CO_2, respectively. Based on the average and maximum concentration ratios of Rn and CO_2 between the two soil gas surveys, it can be inferred that the activities of the Xinbaoan–Shacheng Fault and the northeastern segment of Tanshan Fault are more intense than the other faults and segments in present study, and thus particular attention should be paid to them in the future regarding their seismic hazard. Furthermore, soil type may play an important role in the concentration of different significant gases.

Acknowledgements. We thank the anonymous reviewers for critical comments and suggestions, as well as Bruce D. Malamud for editorial handling. This work was financially supported by the Basic Research Project of Institute of Earthquake Science, China Earthquake Administration (grant no. 02132420, 0213241503). We thank Xiaoqiang Li for his help with sample collection and measurement in field work.

Edited by: B. D. Malamud
Reviewed by: two anonymous referees

References

Al-Hilal, M. and Al-Ali, A.: The role of soil gas radon survey in exploring unknown subsurface faults at Afamia B dam, Syria, Radiat. Meas., 45, 219–224, 2010.

Annunziatellis, A., Beaubien, S. E., Bigi, S., Ciotoli, G., Coltella, M., and Lombardi, S.: Gas migration along fault systems and through the vadose zone in the Latera caldera (central Italy): Implications for CO_2 geological storage, Int. J. Greenhouse Gas Control., 2, 353–372, 2008.

Baubron, J. C., Rigo, A., and Toutain, J. P.: Soil gas profiles as a tool to characterize active tectonic areas: the Jaut Pass example (Pyrenees, France), Earth. Planet. Sci. Lett., 196, 69–81, 2002.

Buringh, P.: Organic carbon in soils of the world: The Role of Terrestrial Vegetation in the Global Carbon Cycle, Measurement by Remote Sensing, Scope Ser., 23, 91–109, 1984.

Camarda, M., De Gregorio, S., and Gurrieri, S.: Magma-ascent processes during 2005–2009 at Mt. Etna inferred by soil CO_2 emissions in peripheral areas of the volcano, Chem. Geol., 330–331, 218–227, 2012.

Ciotoli, G., Guerra, M., Lombardi, E., and Vittori, E.: Soil gas survey for tracing seismogenic faults: a case study in the Fucino basin, Central Italy, J. Geophys. Res., 103, 23781–23794, 1998.

Ciotoli, G., Lombardi, S., and Annunziatellis, A.: Geostatistical analysis of soil gas data in a high seismic intermontane basin: Fucino Plain, central Italy, J. Geophys. Res., 112, B05407, doi:10.1029/2005JB004044, 2007.

Choubey, V. M., Bist, K. S., Saini, N. K., and Ramola, R. C.: Relation between soil-gas radon variation and different lithotectonic units, Garhwal Himalaya, India. Appl. Radiat. Isot., 51, 587–592, 1999.

Earthquake Disaster Defense department of CEA: Chinese historical strong earthquake catalog (The 23rd century BC-1911 AD), Seismological Press, Beijing, 1995 (in Chinese).

Elkins, T. A.: The reliability of geophysical anomalies on the basis of probability considerations, Geophysics, 5, 321–336, 1940.

FAO/IIASA/ISRIC/ISSCAS/JRC: Harmonized World Soil Database (version 1.2), FAO, Rome, Italy and IIASA, Laxenburg, Austria, 2012.

Faulkner, D. R., Jackson, C. A. L., Lunn, R. J., Schlische, R. W., Shipton, Z. K., Wibberley, C. A. J., and Withjack, M. O.: A review of recent developments concerning the structure, mechanics and fluid flow properties of fault zones, J. Struct. Geol., 32, 1557–1575, 2010.

Fu, C. C., Yang, T. F., Walia, V., and Chen, C. H.: Reconnaissance of soil gas composition over the buried fault and fracture zone in southern Taiwan, Geochem. J., 39, 427–439, 2005.

Fu, C. C., Yang, T. F., Du, J., Walia, V., Chen, Y. G., Liu, T. K., and Chen, C. H.: Variations of helium and radon concentrations in soil gases from an active fault zone in southern Taiwan, Radiat. Meas., 43, S348–S352, 2008.

Gal, F., Joublin, F., Haas, H., Jean-Prost, V., and Ruffier, V.: Soil gas (^{222}Rn, CO_2, ^{4}He) behaviour over a natural CO_2 accumulation, Montmiral area (Drôme, France): geographical, geological and temporal relationships, J. Environ. Radioact., 102, 107–118, 2011.

Gao, W. X. and Ma, J.: Seismic geological environment and seismic hazard in the capital area, Seismological Press, Beijing, 1993 (in Chinese).

Ghosh, D., Deb, A., Sengupta, R., Bera, S., Sahoo, S. R., Haldar, S., and Patra, K. K.: Comparative study of seismic surveillance on radon in active and non-active tectonic zone of West Bengal, India, Radiat. Meas., 46, 365–370, 2011.

Guo, H., Jiang, W. L., and Xie, X. S.: Late-Quaternary strong earthquakes on the seismogenic fault of the 1976 $M_S = 7.8$ Tangshan earthquake, Hebei, as revealed by drilling and trenching, Sci. China. Earth. Sci., 54, 1696–1715, doi:10.1007/s11430-011-4218-x, 2011.

Hinkle, M. E.: Environmental conditions affecting concentrations of He, CO_2, O_2 and N_2 in soil gases, Appl. Geochem., 9, 53–63, 1994.

Huang, J. L. and Zhao, D. P.: Crustal heterogeneity and seismotectonics of the region around Beijing, China, Tectonophysics, 385, 159–180, 2004.

Jiang, W. L., Hou, Z. H., Xiao, Z. M., and Xie, X. S.: Study on Paleoearthquakes of Qixinzhuang trench at the Xiadian Fault, Beijing plain, Seism. Geol., 22, 413–422, 2000 (in Chinese).

King, C. Y.: Gas geochemistry applied to earthquake prediction: An Overview, J. Geophys. Res., 91, 12269–12281, 1986.

Kumar, A., Singh, S., Mahajan, S., Bajwa, B. S., Kalia, R., and Dhar, S.: Earthquake precursory studies in Kangra valley of North West Himalayas, India, with special emphasis on radon emission, Appl. Radiat. Isot., 67, 1904–1911, 2009.

Li, L., Chen, Q. F., Cheng, X., and Niu, F. L.: Spatial clustering and repeating of seismic events observed along the 1976 Tangshan fault, north China, Geophys. Res. Lett., 34, L23309, doi:10.1029/2007GL031594, 2007.

Li, Y., Du, J. G., Wang, F. K., Zhou, X. C., Pan, X. D., and Wei, R. Q.: Geochemical characteristics of soil gas in the Yanhuai basin, northern China, Earthq. Sci., 22, 93–100, 2009.

Li, Y., Du, J. G., Wang, X., Zhou, X. C., Xie, C., and Cui, Y. J.: Spatial variations of soil gas geochemistry in the Tangshan area, Northern China, Terr. Atmos. Ocean. Sci., 24, 323–332, 2013.

Lombardi, S. and Voltattorni, N.: Rn, He and CO_2 soil gas geochemistry for the study of active and inactive faults, Appl. Geochem., 25, 1206–1220, 2010.

Menetrez, M. Y. and Mosley, R. B.: Evaluation of radon emanation from soil with varying moisture content in a soil chamber, Environ. Int., 22, Suppl. 1, S447–S453, 1996.

Pavlides, S. B., Zouros, N. C., Fang, Z. J., Cheng, S. P., Tranos, M. D., and Chatzipetros, A. A.: Geometry, kinematics and morphotectonics of the Yanqing–huailai active faults (Northern China), Tectonophysics, 308, 99–118, 1999.

Ran, Y. K., Deng, Q. D., Yang, X. P., Zhang, W. X., Li, R. C., and Xiang, H. F.: Paleoearthquakes and recurrence interval on the seismogenic fault of 1679 Sanhe–Pinggu $M_S = 8.0$ earthquake Hebei and Beijing, Seism. Geol., 19, 193–201, 1997 (in Chinese).

Seismic geological brigade, China Earthquake Administration: The systematic active tectonic map in Beijing area, China printing plant, Shanghai, 1979 (in Chinese).

Seminsky, K. Zh. and Demberel, S.: The first estimations of soil–radon activity near faults in Central Mongolia, Radiat. Meas., 49, 19–34, 2013.

State Seismological Bureau: Tangshan earthquake of 1976, Seismology Publisher, Beijing, 1982 (in Chinese).

Toutain, J. P. and Baubron, J. C.: Gas geochemistry and seismotectonics: a review, Tectonophysics, 304, 1–27, 1999.

Walia, V., Mahajan, S., Kumar, A ., Singh, S., Bajwa, D. S., Dhar, S., and Yang, T. F.: Fault delineation study using soil-gas method in the Dharamsala area, NW Himalayas, India, Radiat. Meas., 43, S337–S342, 2008.

Walia, V., Lin S. J., Fu, C. C., Yang, T. F., Hong, W. L., Wen, K. L., and Chen, C. H.: Soil-gas monitoring: A tool for fault delineation studies along Hsinhua Fault (Tainan), Southern Taiwan, Appl. Geochem., 25, 602–607, 2010.

Walia, V., Yang, T. F., Lin, S. J., Kumar, A., Fu, C. C., Chiu, J. M., Chang, H. H., Wen, K. L., and Chen, C. H.: Temporal variation of soil gas compositions for earthquake surveillance in Taiwan, Radiat. Meas., 50, 154–159, doi:10.1016/j.radmeas.2012.11.007, 2012.

Wang, J., Liu, Q. Y., Chen J. H., Li, S. C., Guo, B., and Li, Y.: The crustal thickness and Poisson's ratio beneath the Capital Circle Region, Chin. J. Geophys., 52, 57–66, 2009 (in Chinese).

Wang, X., Li, Y., Du, J., Zhou, X.: Correlations between radon in soil gas and the activity of seismogenic faults in the Tangshan area, North China, Radiat. Meas., 60, 8–14, 2014.

Xu, X. W., Ji, F. J., Yu, G. H., Chen, W. B., Wang, F., and Jiang, W. L.: Reconstruction of paleoearthquake sequence using stratigraphic records from drill logs: a study at the Xiadian Fault, Beijing, Seism. Geol., 22, 9–19, 2000 (in Chinese).

Xu, X. W., Wu, W. M., Zhang, X. K., Ma, S. L., Ma, W. T., Yu, G. H., Gu, M. L., and Jiang, W. L.: New Crustal Structure Motion and Earthquake in Capital Area, Science Press, Beijing, 2002 (in Chinese).

Yang, T. F., Walia, V., Chyi, L. L., Fu, C. C., Chen, C. H., Liu, T. K., Song, S. R., Lee, C. Y., and Lee, M.: Variations of soil radon and thoron concentrations in a fault zone and prospective earthquakes in SW Taiwan, Radiat. Meas., 40, 496–502, 2005.

Yin, B. J.: Dynamic characteristics of underground water in the Tangshan well, Ph.D. thesis, Institute of Geophysics, China Earthquake Administration, China, 37–38, 2010 (in Chinese).

Zhang, X. K., Zhao, J. R., Liu, G. H., Song, W. R., Liu, B. J., Zhao, C. B., Cheng, S. X., Liu J. D., Gu, M. L., and Sun, Z. G.: Study on fine crustal structure of the Sanhe-Pinggu Earthquake (M = 8.0) region by deep seismic reflection profiing, Earthq. Res. China., 18, 326–336, 2002 (in Chinese).

Zhou, X. C., Du, J. G., Chen, Z., Cheng, J. W., Tang, Y., Yang, L. M., Xie, C., Cui, Y. J., Liu, L., Yi, L., Yang, P. X., and Li, Y.: Geochemistry of soil gas in the seismic fault zone produced by the Wenchuan $M_S = 8.0$ earthquake, southwestern China, Geochem. Trans., 11, doi:10.1186/1467-4866-11-5, online first, 2010.

Zhu, H. S., Zhao, C. M., Li, G. H., Xue, Z. F., and Jiang, W.: Tectonic characteristics of Yanhuai basin and evaluation of potential seismic risk, North. China, Earthq. Sci., 24, 38–42, 2006 (in Chinese).